

EXPERIMENTAL TESTING OF A SMART LEADING EDGE HIGH LIFT DEVICE FOR COMMERCIAL TRANSPORTATION AIRCRAFTS

Markus Kintscher, Hans Peter Monner, Olaf Heintze
DLR

Keywords: *morphing, leading edge, adaptronic, high-lift, droop nose*

Abstract

In the projects SmartLED and SADE a smart droop nose concept for a commercial transportation aircraft is developed by the partners EADS-IW, EADS-MAS and the DLR. The objective is a gap and step-less high lift device for the next generation aircraft of high surface quality for drag reduction. The paper is focused on the preliminary experimental testing of a small section of a full-scale smart leading edge structure which is about to be tested in a ground test in the framework of the project SmartLED. The results of the experimental testing i.e. deformations of the structure and strains are compared to predictions from FE analyses of droop angles of 5°, 10° and 16°.

1 Introduction

To meet the ambitious goals defined in the VISION 2020, technologies to consequently reduce drag and airframe noise will be necessary. The ambitious recommendations of the ACARE group for the reduction of emissions per passenger kilometers are CO₂ < 50%, NO_x < 80% and noise < 50% until 2020. Therefore new aircraft concepts and with it new concepts for high lift devices have to be developed. The developed systems have to comply with the next generation aircraft requirements like high surface quality and lightweight design. In conventional high lift configurations, devices on leading and trailing edges open slots to achieve the additional lift. However, the slots and especially slat gaps at the leading edge have been identified as the dominant source of airframe noise in approach. In the DLR project LEISA different high lift

devices were investigated in an interdisciplinary way for the assessment of high lift system design for low noise exposing high lift devices [1]. Although there is a chance to reduce the slat noise by re-arranging the slat gap in combination with an increased chord slat, nevertheless the slots remaining in the airfoil do not comply with requirements for high quality surfaces for future aircraft airfoil design. Regarding the objective of drag reduction, most experts agree that laminarization is the only technology which has the potential for step changes in drag reduction within a suitable timeframe. Current projects dealing with laminar flow research activities like TELFONA, show promising results for drag reduction up to -12% for the wing [2]. Thus, it is probable that the next generation of wings will employ high aspect-ratios with slim profiles and high quality surfaces like already investigated e.g. within the project NACRE under the acronym HARLS (High Aspect-Ratio Low Sweep) [3].

Because of the gap which forms between the slat and the main wing when deployed, the flow at conventional high lift devices is disturbed and causes transition to turbulent flow immediately after the slat gap. Additionally, the construction space in the next generation high aspect ratio wings is limited due to the employment of slim profiles.

Thus, smart seamless and gapless high lift devices especially at the wings leading edge are a mandatory enabler for future wings of significantly increased aerodynamic efficiency and reduced acoustic intensity. The European and national projects SADE (Smart High Lift Devices for Next Generation Wings) and SmartLED (Smart Leading Edge Device) as well as part of the European funded Clean Sky

Initiative SFWA (Smart Fixed Wing Aircraft) thus aim at a major step forward in the development and evaluation of the potential of morphing airframe technologies.

In the project SmartLED a full-scale demonstrator of 2m span is in preparation for a ground test including tests of leading edge droop and superimposed wing bending deformation with the partners Airbus, EADS-IW and EADS-MAS. This paper focuses on a preliminary test of a small section of the leading edge structure developed within the SmartLED project. Main issue is a first-time comparison of FE analysis results with measured deformation and strains of the deformed leading edge structure.

2 Description of the Smart Droop Nose Concept

The concept of the smart leading edge device in the SmartLED project is based on the patent DE 2907912-A1 which was invented at the Dornier Company in the year 1979 (Fig. 1)[4].

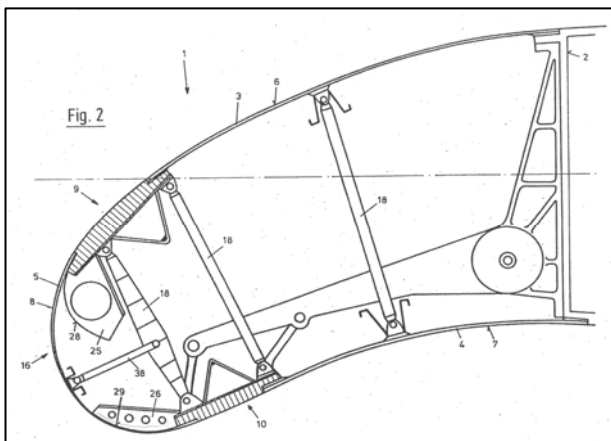


Fig. 1. Patent DE2907912-A1, Dornier Company, 1979.

The Dornier concept assumes a main lever attached to the front spar which serves as main actuation mechanism and deforms the structure consisting of several flexible panels. The flexible panels are attached to the inner mechanism in a way that the contour is continuously closed and the inner mechanism guides the movement of the structure to the

desired shape with an increasing nose radius. A variety of patents describing droop nose concepts can be found from which the most are focused on an inner mechanism providing the movement and support of a not otherwise specified skin structure. Nevertheless, the patent DE 2907912-A1 was selected in concept phase due to its best conformity with the challenging industrial requirements in the project.

Concerning the actuation of the smart leading edge the idea of a main lever driven by a rotational actuator as well as the connection of the skin to the main lever by several small struts is adopted. The direct connection of the upper and lower skin is neglected in this preliminary design to eliminate deformation constraints. Due to the high demands on the surface quality of such a device all connections concerning the skin must be realized without riveting. As well the concept of individual skin panels attached to the inner mechanism is not feasible due to the gaps and steps at the panel joints. Therefore an approach for continuously integrally manufactured skin/interface-structure is followed. Within this approach the concept utilizes omega shaped stiffeners for the load transfer from the actuation over the main lever to the skin and for the transfer of the aerodynamic loads into the front spar. The omega shaped stringers have the advantage that besides forces moments can be transmitted into the skin. This provides an additional parameter for the designer to achieve a desired target shape. In the same way the large surface of the omega-stringer foot is an advantage in the design of the stringers connected to the upper skin. There the aerodynamic load results in a peel off loading of the stringer foot for which the only solution is a suitable design of the glued surface. In case of stability problems in span wise direction for example in wing bending tests the stringers can be filled with foam to increase the bending stiffness in span direction. In Fig. 2 the smart droop nose concept in the national project SmartLED is outlined. With a leading edge chord of about 600mm and a front spar height of about 370mm the section corresponds to a leading edge outboard section of an A320 wing near the kink.

The crucial point in the design of a smart leading edge is the design of the skin stiffness distribution for a desired aerodynamic target shape. In order to get as close as possible to an aerodynamic target shape the design process has to consider all given boundary conditions for the skin and the actuation mechanism in one optimization loop.

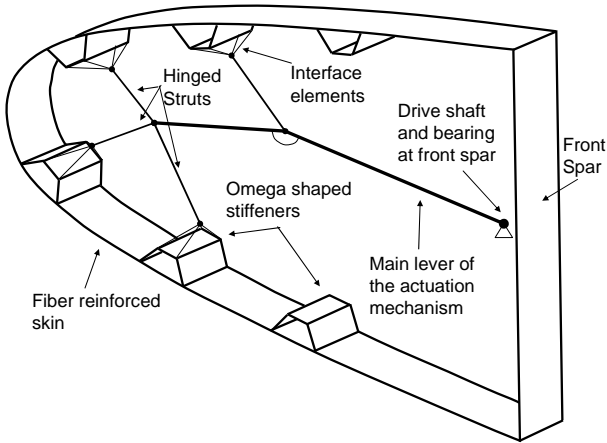


Fig. 2. Smart Droop Nose Concept in the national LuFo IV project SmartLED.

3 Design of the Smart Leading Edge

For the design of the smart leading edge structure a full parametric design cycle is used. Due to the strong coupling of structure and kinematics regarding the target shape an overall finite element model consisting of structure and kinematics is mandatory for the design and optimization of the smart leading edge structure. As well the consideration of common boundary conditions of both, structure and kinematics is easier. In the design cycle all necessary design steps for design and optimization are covered starting from an initial skin design, the calculation of number and position of support stations, the detailed design of the skin comprising for example the layup sequence and layer orientation angle to the point of pre-design and integration of a suitable actuation mechanism for the gathering of first characteristic actuation data.

In the first step the given aerodynamic input shape of the airfoil during cruise flight and the shape in approach are analyzed. From this analysis a first skin thickness distribution t can be obtained due to the direct relation of linearized strain, difference in curvature and the local skin thickness. In equation 1 a limit strain value is used to calculate a preliminary skin thickness distribution $t(s)$ along the circumferential length s of the nose profile as input data for the design loop.

$$t(s) = 2 \cdot \varepsilon_{\text{lim}} \cdot \frac{1}{\Delta\kappa(s)} \quad (1)$$

With the preliminary skin thickness distribution the design cycle can be started. Within the design cycle the number and position of support points as well as a detailed stiffness distribution of the skin for a given target shape is assessed by an iterative optimization procedure. This includes the calculation of the cruise shape and the drooped shape with the corresponding aerodynamic loads in every step of the iteration. In the next phase the finite element model in the design cycle is complemented with a pre-designed actuation mechanism for a coupled simulation of kinematics and the smart structure and a second more detailed optimization loop is used.

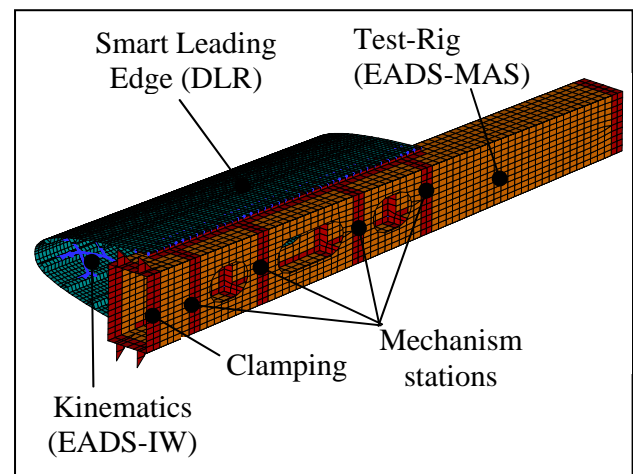


Fig. 3. FE model of the test-rig including smart leading edge structure and kinematics for system simulation, [5].

A detailed description of the design methodology and optimization loops can be found in [5]. In Fig. 3 an overall finite element model including the smart leading edge structure, actuation mechanism, and the experimental test-rig is shown. It is created using the design cycle in preparation of the planned ground test for the virtual demonstration of the complete system.

4 Experimental tests and comparison with FE analysis results

The 25mm wide section described in Fig. 4 is obtained as a slice of the 2m test section for the ground test presented in Fig. 3. In advance of the ground test of the leading edge test structure especially the consistency of the deformation behavior of the finite element modeling and the manufactured structure is of interest.

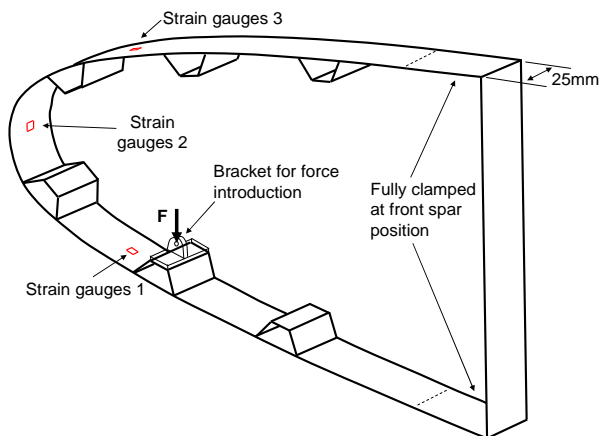


Fig. 4. Test section with position of strain gauges for measurements.

For a consistency check a finite element model of the 25mm wide section is created using the tools for parametric modeling from the process chain for the design of the smart leading edge structure described in the previous chapter. In the deformation tests the denoted actuation mechanism in Fig. 2 is replaced and for simplification the deformation is induced by applying a force directly to the first load introduction stringer near strain gauge 1 on the lower skin at a bracket. Three different forces

for the deformation of the structure are applied to the bracket by weights in steps of 2kg. During the measurements the structure is fully clamped at the position where normally the structure would be attached to the front spar at a length of 80mm. For the measurements strain gauges are positioned at three locations of the profile. The strain gauges one and two are located at position of the maximum change of curvature between the cruise and the drooped shape. The critical strains in circumferential direction are therefore intended to be measured at these positions. Especially the strain at the position of strain gauge one is predicted as the most critical for the structure. Strain gauge three is located on the upper skin in a region where more moderate strains are assumed. The strain gauges at all positions are used in half-bridge configuration for the measurement of pure bending strains.

For the measurement of the deformed shape of the structure a picture is taken from the undeformed and deformed structure every load step with a camera. Then the shape is extracted with an imaging toolbox by a digitizer and transformed into the coordinate system of the finite element model by translation and rotation.

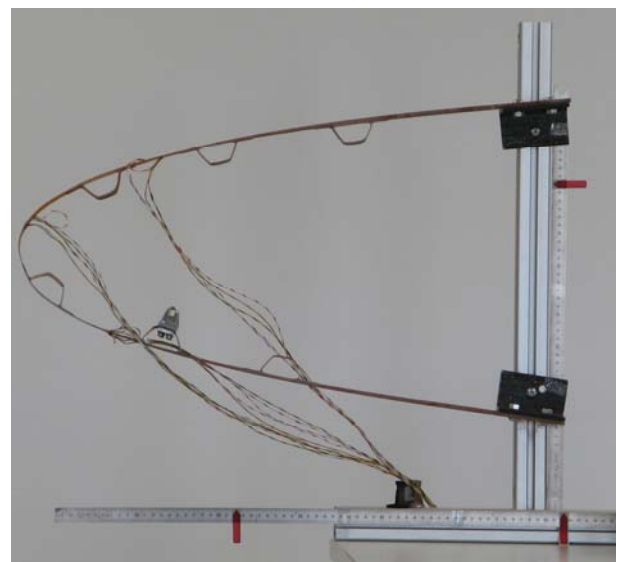


Fig. 5. Test section in undeformed position

For the shape comparison the undeformed structure is taken as reference and the transformation rule for translation and rotation

is determined and used for all following transformations.

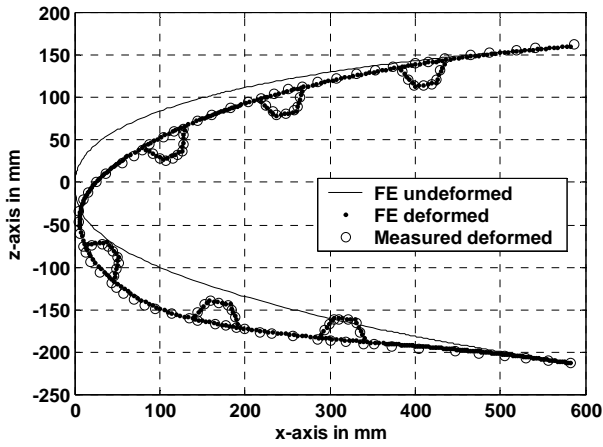


Fig. 6. Comparison of shapes in drooped position with 5° droop angle.

In the first load step a weight of 2kg is applied to the structure. The resulting deformation of the structure represents a droop angle of the nose section of 5° with a maximum deformation in loading z-direction of 45mm. The shape comparison of the FE analysis and the measurements is shown in Fig. 6. The shapes are in good agreement over the complete circumferential length of the nose profile.

For the applied deformation the strains in circumferential direction are predicted with a maximum strain of 0.31% in the outer layer just after the stringer foot at the edge of the section as shown in Fig. 7.

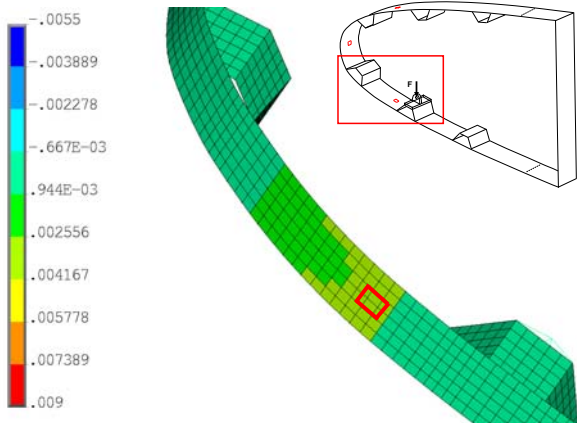


Fig. 7. Strain at 5° droop angle and position of strain gauge one; Max. strain 0.31% in circumferential direction of the outer layer.

The maximum strain at this location results from a large change of the bending stiffness due to the ending of the layers which form the stringer foot of the load introduction stringer and the load for the deformation which is transferred at this point to the structure.

For the next load steps of 4kg and 6kg the comparison of the shapes at 10° and 16° droop angle shows a good agreement of the predicted and measured shape of the smart droop nose structure for larger droop angles too (Fig. 8 and Fig. 9).

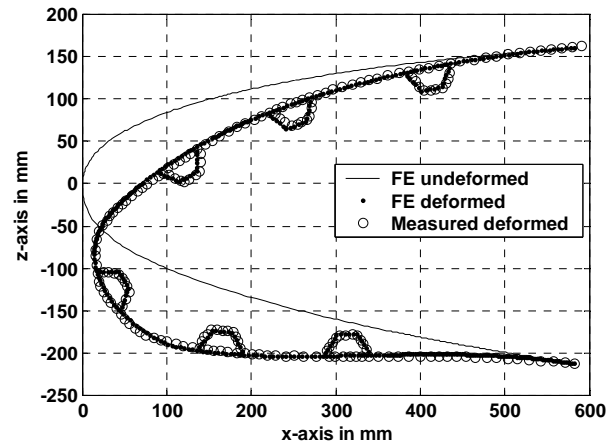


Fig. 8. Comparison of shapes in drooped position with 10° droop angle.

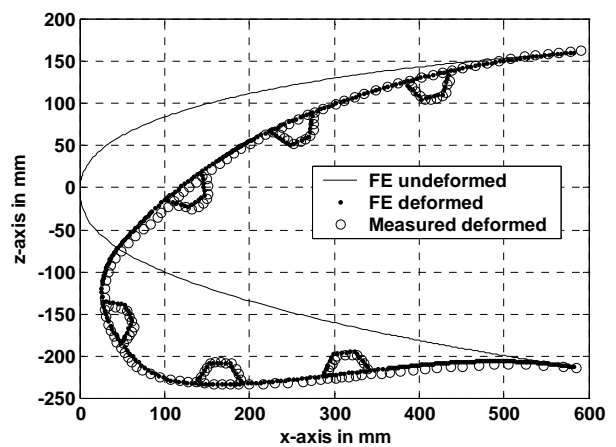


Fig. 9. Comparison of shapes in drooped position with 16° droop angle.

Concerning the comparison of strains for these load steps a large difference of the measured and predicted circumferential strain at the position of strain gauge one can be noticed. In Fig. 10 and Fig. 11 the distribution of the strain in circumferential direction of the outer layer is shown for the corresponding load respectively. For both loadings the predicted maximum strain at the specified location exceeds the measured strain.

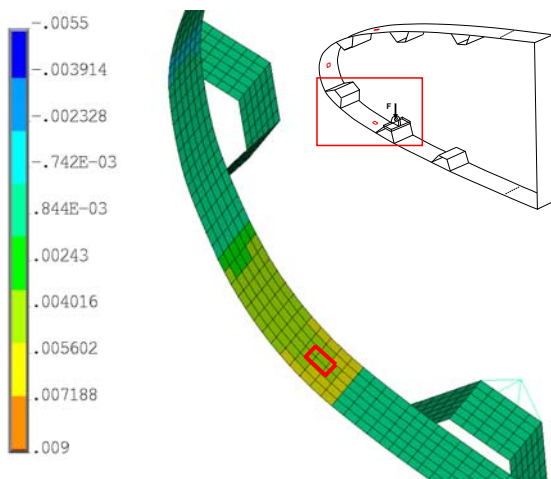


Fig. 10. Strain at 10° droop angle and position of strain gauge one; Max. strain of 0.6% in circumferential direction of the outer layer.

A summary of the measured strains at the three locations of the strain gauges is given in Fig. 12.

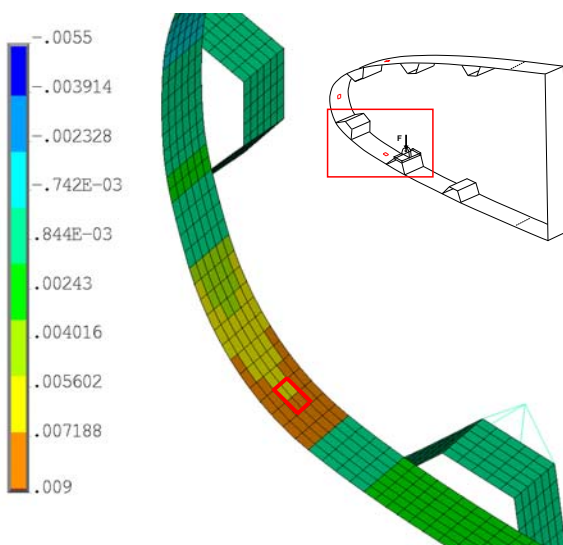


Fig. 11. Strain at 15° droop angle and position of strain gauge one; Max. strain of

0.9% in circumferential direction of the outer layer.

The reason for the mismatch of the strain values at position one is presumably a deviation of the skin thickness in the finite element model due to the discretization. Fig. 13 shows a crosscheck of the expected strains by analytical calculated strains.

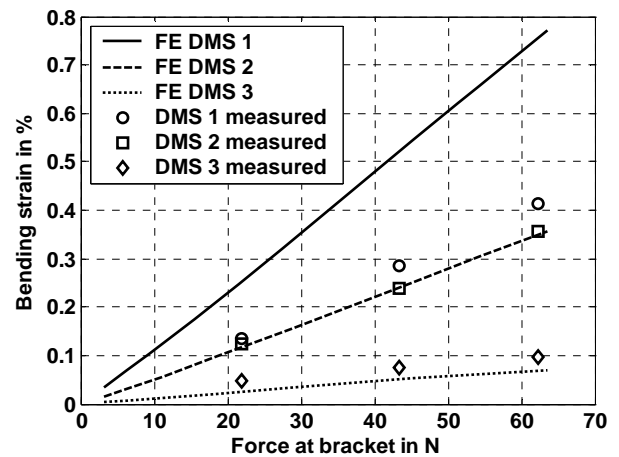
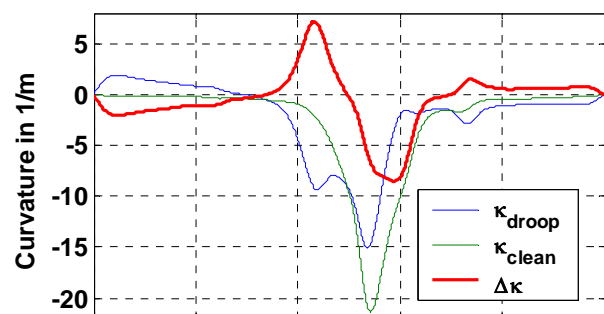


Fig. 12. Comparison of predicted and measured strain

For reference the strains in this plot are calculated with eq. 1 analytically from the difference in curvature between the shapes and the measured and interpolated skin thickness along the profiles circumference. In the strain plot of Fig. 13 the maximum strains are around $\pm 0.5\%$ which is in good agreement with the maximum measured strains at the position of strain gauge one of $\pm 0.42\%$.



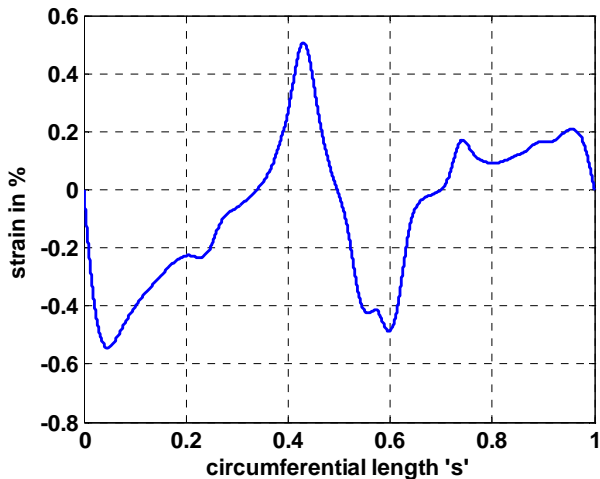


Fig. 13. Analytical calculated strain and curvature along the circumferential length s .

6 Conclusions

In the national project SmartLED a smart droop nose concept for commercial transportation aircrafts is developed by the DLR, EADS-IW and EADS-MAS. The presented paper focuses on the experimental testing of a small section of a 2m span section of a smart droop nose structure which is about to be tested in a ground test at EADS-MAS including tests under wing bending. From the experimental testing of the structure the deformed shape and the strains are compared to the shapes under loading and the predicted strains. It was found that the parametric modeling with the underlying process chain for the design of the smart droop nose device is well suited to predict the deformation behavior even at large deformations. The evaluation of the calculated and measured strains showed significant differences in the maximum strain in the nose tip. In a crosscheck the strains are calculated from the curvature difference of the shapes and the measured skin thickness. Thereby it could be shown that the strains in the FE analysis are over estimated due to the used discretization and inconsistency of the skin thickness.

7 Acknowledgements

The presented results are part of the work in the national LuFo IV project SmartLED and the project SADE which is part of the 7th European Framework Program for research in aeronautics.

The author is appreciative for the support and cooperation of the work by the project partners EADS Innovation Works and EADS Military Air Systems.

References

- [1] Wild, J., Pott-Pollenske, M., Nagel, B.: "An integrated design approach for low noise exposing high lift devices. AIAA-2006-2843, 2006.
- [2] Horstmann, K. H.: "TELFONA, Contribution to Laminar Wing Development for Future Transport Aircraft", Aeronautical Days, Vienna, 19th-21st June 2006.
- [3] Laban, M., Maseland, J. E. J., Kok, J. C., Jentkin, H. W., Brouwer, H. H.: "Reducing Aircraft Emissions; The NACRE Pro-Green Aircraft Concept Study", 2nd NACRE workshop 2008, 10-11 July 2008, London, Greenwich.
- [4] Zimmer, H.: "Quertriebskörper mit veränderbarer Profillierung, insbesondere Flugzeugtragflügel", German Patent No. DE 2907912 -A1, 1979.
- [5] Kintscher, Markus. "Method for the Pre-Design of a Smart Droop Nose using a Simplex Optimization Scheme". SAE Aerotech Congress and Exhibition , 10.-12. November 2009 , Seattle, Washington, USA.

8 Contact Author Email Address

Dipl.-Ing. Markus Kintscher

Institute of Composite Structures and Adaptive Systems
 German Aerospace Center, DLR
 Lilienthalplatz 7
 38108 Braunschweig
 Phone: +49 531 295 3046
Markus.Kintscher@dlr.de

Copyright Statement

The authors confirm that they, and/or their company or organization, hold copyright on all of the original material included in this paper. The authors also confirm that they have obtained permission, from the copyright holder of any third party material included in this paper, to publish it as part of their paper. The authors confirm that they give permission, or have obtained permission from the copyright holder of this paper, for the publication and distribution of this paper as part of the ICAS2010 proceedings or as individual off-prints from the proceedings.